



Elastic energy of the discocyte–stomatocyte transformation

S. Muñoz^{*}, J.L. Sebastián, M. Sancho, G. Álvarez¹

Departamento de Física Aplicada III, Facultad de Ciencias Físicas, Universidad Complutense, 28040 Madrid, Spain

ARTICLE INFO

Article history:

Received 12 June 2013

Received in revised form 10 October 2013

Accepted 28 October 2013

Available online 2 November 2013

Keywords:

Red blood cell shape

Discocyte–stomatocyte sequence

Erythrocyte membrane

Bending energy

ABSTRACT

The aim of this study is to calculate the membrane elastic energy for the different shapes observed in the discocyte–stomatocyte sequence. This analysis can provide a better quantitative understanding of the hypothesis put forward over the last decades to explain how red blood cells produce and maintain their typical shape. For this purpose, we use geometrical models based on parametric equations. The energy model considered for the elastic properties of RBC membrane includes the local and nonlocal resistance effects of the bilayer to bending. In particular, the results confirm the discocyte as the lowest energy value configuration among the sets of different red blood cell deformations considered in the sequence.

© 2013 Elsevier B.V. All rights reserved.

1. Introduction

Over the last decades many studies have focused on the mechanical and rheological properties that determine the biological function of the red blood cells (RBCs) [1 and therein]. These properties seem to be closely related to the normal RBC biconcave disc shape (often referred to as discocyte or erythrocyte), with its relatively high surface-to-volume ratio, and ultimately to the RBC flexible membrane. The combined effects of the phospholipid bilayer and of the underlying membrane skeleton determine the elastic and biorheological properties that allow RBCs to pass through small capillaries during microcirculation. Several hypotheses have been put forward to explain how the cell produces and maintains its resting biconcave shape. These hypotheses include elastic forces within the membrane, surface tension, electrical forces on the membrane surface and osmotic or hydrostatic pressures [2]. It is also well known that pathological conditions or treatment *in vitro* with a variety of amphipathic agents transforms systematically and reversibly the normal biconcave shape into less symmetric shapes such as the stomatocytes [3] or even into non-axisymmetric biconcave shapes [4], and several theoretical and experimental studies [5–10] suggest that among the variety of effects previously mentioned, the elastic bending energy is the dominant factor that determines the equilibrium shape of the membrane (i.e., its energetically more favorable configuration). Since the original works of Canham [11] and Lew [12], energy models that included spontaneous curvature and the

contribution of bilayer couple (as well as more geometrically accurate cell descriptions) have been developed to study the different cell shapes observed in many experiments [13–16]. These previous studies showed comparisons of elastic energy between some observed and proposed cell shapes. However, we are not aware of any quantitative study of the elastic energy stored on the membrane for the great variety of observed RBC reversible deformations. The purpose of this work is to present such a systematic quantitative analysis of the energy associated to the basic and altered RBC cell geometric shapes (including those with no rotational or axial symmetry that have not been studied so far) without invoking the full bioelectrochemistry of cells. This study may be very useful to estimate the order of magnitude of the force needed to induce specific RBC shapes in procedures such as micropipette aspiration or laser tweezers techniques [17].

A key issue to achieve this goal is to select a suitable compromise between accuracy of the geometrical representation of the cell shapes and complexity of the geometrical model itself (i.e., how can be obtained and controlled the desired deformations) and of the ensuing elastic energy calculations. Early geometrical models for the normal erythrocyte consisted of surfaces of revolution generated by Cassini curves. The main advantage of this representation is that Cassini curves admit parameterizations in terms of trigonometric functions; the main limitation is that Cassini curves are determined by only two parameters, which can be used to fix, say, only the length and the height of the erythrocyte. One possibility to overcome this limitation is to expand the shape profile into a Fourier series [18], and use as many Fourier coefficients as needed to reach a certain prescribed accuracy. At the other extreme, purely numerical methods (in which the surface is discretized) and variational algorithms can be used to calculate the optimal bending energies and shapes [19]. These methods can achieve a very high precision because, in effect, the discretization vertices provide a large number of

^{*} Corresponding author. Tel.: +34 1 3944373; fax: +34 1 3945196.

E-mail address: smsm@ucm.es (S. Muñoz).

¹ Departamento Física Teórica II, Métodos Matemáticos de la Física, Facultad de Ciencias Físicas, Universidad Complutense, 28040 Madrid, Spain.

parameters. We have opted for an intermediate possibility: we give sufficiently realistic geometrical models that reproduce the morphologic changes of RBCs well documented in the literature but that can be controlled with a small number of parameters. In spite of the interest on the full echinocyte–discocyte–stomatocyte sequence, most studies have calculated the elastic energy only for the left part of this sequence, i.e., the echinocyte–discocyte subsequence. This restriction may be due to the lack of simple parameterizations of the stomatocyte shape that we present in this work. Although it could be argued that the spherical geometry has the lowest energy [20], this spherical shape does not feature the high surface to volume ratio required for the RBC biological function. Nevertheless, we include in our study the sphero-stomatocyte, a quasi-spherical form that is randomly observed in many hematological disorders. The advantage of this approach is twofold: it provides a sufficiently accurate and efficient description of the continuous transformations between normal discocytes and altered shapes, and it accommodates both axisymmetric and non-axisymmetric shapes. Moreover, the use of parametric equations makes easier the calculations of all surface integrals over the two local principal curvatures to determine the membrane elastic energy. Thus, under a geometrical constraint of a constant cell volume ($85 \mu\text{m}^3$) and assuming that the cytoplasm is an incompressible liquid, we determine the elastic energy of different observable RBC shapes by applying the parametric equations to the existing energy models.

The layout of the paper is as follows. In Section 2 we first describe the geometrical models proposed for the different deformations of RBCs. We show how the parametric equations can be modified to describe normal and altered RBCs shapes, in particular cells that show different degrees of invagination (stomatocyte types) or loss of axial symmetry and that to the best of our knowledge have not been studied so far. We use *Mathematica* [21] to generate all the 2D sections and 3D solid models as well as for the calculations of the cell energy. Then we use our parameterizations to calculate in Section 3 the elastic energy for the various geometries appearing in the DS sequence by using the elastic energy model proposed by Canham [11]. Next, we take into account the asymmetry in the bilayer-couple produced by the difference in relaxed areas between the outer and inner leaflets [7,22,23]. For this purpose, we incorporate the spontaneous curvature and the area-difference elasticity as new parameters into the energy analysis. These results show that the effects of the spontaneous curvature and the area difference elasticity are of a great importance on shapes lacking rotational or axial symmetry. Finally, we discuss our results in Section 4.

2. Cell geometric models

2.1. Axisymmetric discocyte model

The biconcave or discocyte shape is the usual and favored RBC shape because its overall membrane energy is a minimum. In previous studies [24–26] we slightly generalized the parametric representation of Kuchel and Fackerell [27] for the normal biconcave discocyte. This parameterization can be written in terms of the Jacobi elliptic functions $\text{sn}(u|m)$, $\text{cn}(u|m)$ and $\text{dn}(u|m)$ with three free parameters:

$$\mathbf{r}_{\pm}(u, \phi) = \left(\frac{\ell}{2} \text{cn}(u|m) \cos \phi, \frac{\ell}{2} \text{cn}(u|m) \sin \phi, \pm h_0 \text{sn}(u|m) \frac{\text{dn}(u|m)}{\text{dn}(U|m)} \right) \quad (1)$$

where ℓ is the diameter of the discocyte, $2h_0$ is the height at its center, $U = K(m)$ is the corresponding complete elliptic integral of the first kind (which satisfies $\text{cn}(U|m) = 0$, $\text{sn}(U|m) = 1$ and $\text{dn}(U|m) = \sqrt{1-m}$, although for clarity we keep the functional form of this last expression in the parametric equations), $u \in [0, U]$, $\phi \in [0, 2\pi]$, and the plus and minus signs correspond to the upper and lower half of

the cell respectively. The only remaining parameter is $m \in [0, 1]$, which we use to fix $2h_{\text{max}}$, the maximum height of the discocyte.

As we mentioned in the Introduction, many experiments have shown that a variety of agents can modify the biconcave shape. The basic hypothesis of the mechanical approach is that the observed RBC shapes are subjected to appropriate constraints on volume and area [7]. However, during the transformation, the RBC surface area decreases more rapidly than its volume, leading to shapes with decreased deformability. In fact, this general idea that the RBC membrane is easily deformed with relatively small changes in area is supported by numerous observations, particularly by sieving tests [28]. The proposed model is able to accommodate changes in the surface area at fixed volume or vice versa. However, since most of the experiments on RBC deformations have been performed keeping constant the tonicity of the suspending medium (so that the cell volume is controlled), except for our comparison with Canham's model [11] in Section 3.1, all the cell models we have considered in our analysis have a fixed total volume of $85 \mu\text{m}^3$, while their surface areas may have different values. The choice of this volume is based on previous studies [29] that showed normal human red cells with average diameters ℓ from 7.5 to 8.3 microns and an average volume of $83 \pm 4 \mu\text{m}^3$.

2.2. Non-axisymmetric discocyte model

Scanning electron microscope images [1] have confirmed a peculiar biconcave shape that either can exist naturally or can be artificially induced. This altered shape, called non-axisymmetric discocyte, can be described as a discocyte with uneven rim thickness, retaining the up-down symmetry of the basic discocyte but having a single additional mirror plane instead of full axial symmetry. This particular shape can be generated by introducing into Eq. (1) two new parameters d and α , see Fig. 1, resulting in the expression.

$$\mathbf{r}_{\pm}(u, \phi) = \left(\frac{\ell}{2} \text{cn}(u|m) \cos \phi, \frac{\ell}{2} \text{cn}(u|m) \sin \phi, \pm \left(\frac{\ell}{2} \text{cn}(u|m) \cos \phi + d \right) \tan(\alpha) \frac{h}{2h_{\text{max}}} \text{sn}(u|m) \frac{\text{dn}(u|m)}{\text{dn}(U|m)} \right) \quad (2)$$

Note that d must be greater than $\ell/2$ and that to keep the volume constant we must take $d = h_{\text{max}}/(2 \tan(\alpha))$. Fig. 1 shows 2D vertical symmetry plane sections and 3D models for different values of α . Table 1 shows the various geometrical parameters for axisymmetric, DS sequence, and non-axisymmetric discocytes. Note that, despite the constraint of constant volume, the increment of the surface area of non-axisymmetric discocytes with increasing values of α is not significant.

2.3. Stomatocyte model

The term stomatocyte generally refers to cup-shaped deformations of the basic discocyte induced by some chemical agents such as low pH, cholesterol, depletion or low salt. It has been observed experimentally [1,16,30] that these transformations follow an orderly sequence of changes of area from discocyte to full stomatocyte. At the beginning of this transformation the area increases, but at a certain point the shape of the stomatocyte begins to approach a more spherical appearance, and the area decreases. Stomatocytes are usually classified into three types (I, II and III), all of them with the same cup-like shape but with different degrees of invagination. Previous studies [1] have shown the I–II–III sequence to be reversible, so that removal of the inducing agent or addition of an antagonist agent at stage III can cycle the shapes back through stages II and I.

The upper and lower parts of the stomatocyte present different degrees of concavity. We can model this cup shape by applying independently Eq. (1) to the upper part and to the lower part of the cell with

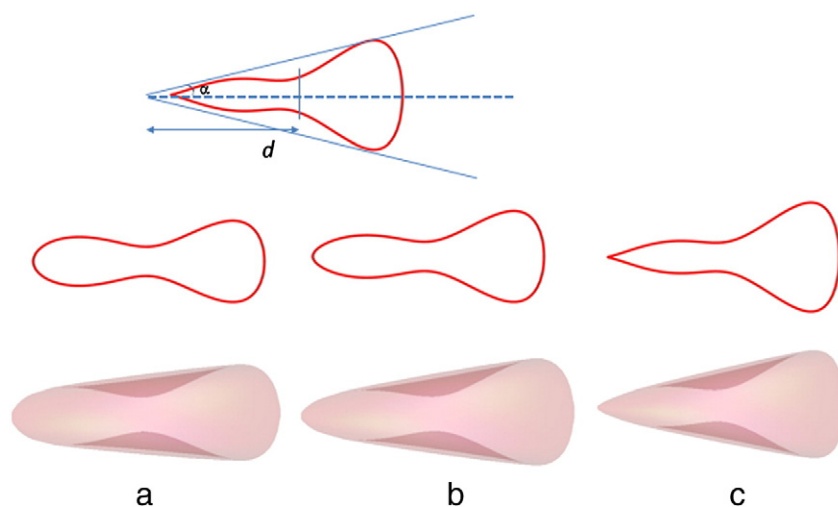


Fig. 1. 2D and 3D models of non-axisymmetric discocyte generated from Eq. (2) with Mathematica for different values of α corresponding to a) $\alpha = \pi/30$, b) $\alpha = \pi/20$, and c) $\alpha = \pi/15$ respectively. The definition of the new parameter d , introduced in the non-axisymmetric discocyte model, is shown in the 2D section.

different parameters ℓ , h_{\pm} , m_{\pm} , $U_{\pm} = K(m_{\pm})$ and different powers (3 and 2 respectively) in the third component:

$$\mathbf{r}_+(u, \phi) = \left(\frac{\ell}{2} \operatorname{cn}(u|m_+) \cos \phi, \frac{\ell}{2} \operatorname{cn}(u|m_+) \sin \phi, h_+ \operatorname{sn}(u|m_+) \times \left(\frac{\operatorname{dn}(u|m_+)}{\operatorname{dn}(U_+|m_+)} \right)^3 \right) \quad (3a)$$

$$\mathbf{r}_-(u, \phi) = \left(\frac{\ell}{2} \operatorname{cn}(u|m_-) \cos \phi, \frac{\ell}{2} \operatorname{cn}(u|m_-) \sin \phi, -h_- \operatorname{sn}(u|m_-) \times \left(\frac{\operatorname{dn}(u|m_-)}{\operatorname{dn}(U_-|m_-)} \right)^2 \right). \quad (3b)$$

The set of Eqs. (3a,3b) can also be used to analyze the evolution from the original discocyte to the final cup shape with a deep invagination. We remark that the two halves of the cell involve different values for the exponent of the Jacobi functions and we refer to Table 1 for the geometrical parameter values of the model at different stages.

Fig. 2 shows 2D and 3D representations of the different types during the discocyte–stomatocyte sequence. These models are in good agreement with RBC scanning electron microscope images of the DS transformation [1,3,16,30].









Table 1 shows, for a fixed cell volume, the surface area along the DS sequence. The sphero-stomatocyte shape, a quasi-sphere that appears at the end of the transition shown in Fig. 2, is a special case that shows a significant decrease of surface area. This peculiar shape presents an irregular surface due to remnants of concavity and, unlike previous stages of the sequence, once reached the quasi-spherical stage the process is not reversible.

3. Elastic energy calculations of altered shapes of RBC: discocyte–stomatocyte transformation

3.1. Zero spontaneous curvature energy model

Early studies of the RBC deformation considered the bounding membrane as a thin, smooth, rotationally symmetric rubber wall whose relaxed state (depending on its surface to volume ratio) was either spherical or a biconcave discoid. However, these studies failed to reproduce various experimental observations. Canham [11] dealt with these discrepancies by considering the membrane to be a two-dimensional fluid bilayer whose curvature elasticity is the shape-controlling factor. In its fluid state [31], it was expected that the RBC membrane would strongly resist changes in overall volume, but any effects related to thickness changes were neglected. The validity of these assumptions was confirmed experimentally by applying tension to membranes

Table 1
Geometric values used in the cell parametric equations.

Cell shape		Diameter l (μm)	Height h (μm) h_+/h_- (μm)	Parameter m m_+/m_-	Surface area A (μm^2)
DS sequence	Sphero-stomatocyte 	5.8	2/2	0.35/0.12	96
	Stomatocyte type III 	6	0.07/2.21	0.94/0.47	116
	Stomatocyte type II 	6.4	0.03/1.48	0.97/0.47	129
	Stomatocyte type I 	7.8	0.05/0.95	0.95/0.47	140
	Discocyte 	7.8	1	0.945	126
Non-axisymmetric shapes	Non-axisymmetric type I ($\alpha = \pi/30$) 	7.8	1	0.945	127
	Non-axisymmetric type II ($\alpha = 1.5\pi/20$) 	7.8	1	0.945	128
	Non-axisymmetric type III ($\alpha = 2\pi/15$) 	7.8	1	0.945	129

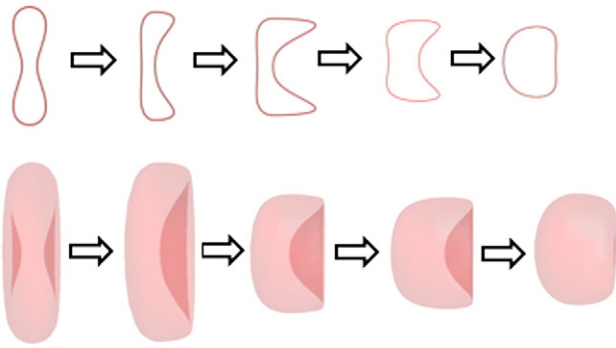


Fig. 2. 2D and 3D models of the DS sequence generated by the set of Eqs. (3a,3b). The figures are shown in the order of appearance in the sequence: discocyte ($l = 7.8 \mu\text{m}$, $h = 1 \mu\text{m}$, $m = 0.945$), stomatocyte I ($l = 7.8 \mu\text{m}$, $h_+ = 0.05 \mu\text{m}$, $h_- = 0.95 \mu\text{m}$, $m_+ = 0.95$, $m_- = 0.47$), stomatocyte II ($l = 6.4 \mu\text{m}$, $h_+ = 0.03 \mu\text{m}$, $h_- = 1.48 \mu\text{m}$, $m_+ = 0.97$, $m_- = 0.47$), stomatocyte III ($l = 6 \mu\text{m}$, $h_+ = 0.07 \mu\text{m}$, $h_- = 2.21 \mu\text{m}$, $m_+ = 0.94$, $m_- = 0.47$) and spherostomatocyte ($l = 5.8 \mu\text{m}$, $h_+ = h_- = 2 \mu\text{m}$, $m_+ = 0.35$, $m_- = 0.12$).

[32–34]. Therefore, bending may be considered responsible of the RBC membrane deformation and the local elastic energy is simply proportional to the surface integral taken over the square of the sum of the two local principal curvatures c_1 and c_2 . The energy is then given by

$$E = \frac{D}{2} \int (c_1 + c_2)^2 dA, \quad (4)$$

where D , the bending rigidity constant, is a function of the thickness of the membrane, of the Young modulus, and of the Poisson ratio. We have first used this simple approximation to check our discocyte geometric model by setting the parameters $l = 8 \mu\text{m}$, $h = 1.032 \mu\text{m}$ and $m = 0.9602$ to reproduce the reference discocyte with a surface area of $137 \mu\text{m}^2$ and a volume of $107 \mu\text{m}^3$ used by Canham. By using the value $D = 4.27 \times 10^{-19} \text{ J}$ proposed by Canham for a membrane thickness of 8 nm , we obtained a discocyte/sphere bending energy ratio of 2.37, which is very similar to the published value of 2.40 [11]. There has been much discussion in the literature about the most suitable value of the elastic constant for the red blood cell membrane. In this paper, as we anticipated in the Introduction, the use of Eq. (4) allows us to assess the importance of including the spontaneous curvature. Therefore, in subsequent calculations we will consider the same value of $D = 2 \times 10^{-19} \text{ J}$ that is used in the non-zero spontaneous curvature energy model [6–8] that we analyze in Section 3.2. The first column in Table 2 shows the bending energy values provided by Eq. (4) for the

discocyte, the different stomatocyte types and the non-axisymmetric models discussed in Section 2 with the geometrical parameters of Table 1.

Our results show that the spherostomatocyte has the lowest energy value, whereas the types I, II, and III stomatocytes feature higher bending energies. The highest bending energy is obtained for the type II stomatocyte. This shape is the last stage that shows an elongated shape. From this point of deformation, the stomatocyte is gradually deformed to a more spherical appearance. This progressive deformation towards a more spherical shape leads to a reduction in the bending energy (see the type III stomatocyte), reaching the minimum value for the last stage of the DS transformation, the spherostomatocyte. Our results are in agreement with the classic study [35] that showed that the spherical shape corresponds to the minimum energy even without fixed volume or surface area constraints. This minimum energy may justify the fact that the spherostomatocyte is an irreversible stage in terms of bending energy. Also, Table 2 shows that the loss of axial symmetry on the discocyte shape leads to a bending energy value that may be even higher than the corresponding to the type II stomatocyte.





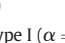



The bending energy defined by Eq. (4) may give a sufficiently accurate value for lipid bilayers consisting of two axisymmetric, homogeneous lipid monolayers and thus be adequate to discuss discocyte and stomatocyte energetics. However, we will show that for the study of shapes with no axial symmetry a more elaborated energy model is required. This expanded model is analyzed in next subsection.

3.2. Non-zero spontaneous curvature energy model

The predictions of the simple energy model for the minimum energy configuration in absence of external forces led to controversial statements about the need for the bilayer to be flat. Helfrich [36] proposed a new description of the free energy of lipid membranes by analogy with a bent box of liquid crystal. This theory viewed the elasticity of lipid bilayers as a special case of the well-established theory of thin elastic shells. This extended energy model includes a spontaneous curvature that can be estimated by treating the monolayer as two surfaces, corresponding one to the headgroup and the other to the acyl chain region [37,38]. This curvature accounts for the asymmetrical chemical or physical interactions between the two leaves of the lipid bilayer. Therefore, a bilayer membrane will exhibit a spontaneous curvature if the two monolayers consist of lipids with different shapes or if the two membrane leaflets are exposed to different chemical environments. Experimental studies showed the combined effects of urea and lysophosphatidylcholine (LPC) on red blood cell shape. The outcome of these treatments evidenced either a change of the naturally preferred curvature of the surface, due to the different headgroup size in

Table 2

Bending energy, spontaneous curvature (c_0), non-zero bending energy and area difference (ΔA) for the DS sequence and the non-axisymmetric shapes randomly observed.

Cell shape		Bending energy ($\times 10^{-18} \text{ J}$)	Spontaneous curvature c_0 (μm^{-1})	Non-zero bending energy ($\times 10^{-18} \text{ J}$)	ΔA (μm^2)	$\Delta A/\Delta A_0$
Axisymmetric shapes DS sequence	Spherostomatocyte 	6.08	0.73	0.94	0.21	0.85
	Stomatocyte type III 	16.53	0.64	11.78	0.22	0.89
	Stomatocyte type II 	20.55	0.59	16.06	0.23	0.93
	Stomatocyte type I 	15.18	0.61	10.05	0.25	1.01
	Discocyte 	9.43	0.66	4.00	0.25	1
Non-axisymmetric shapes	Non-axisymmetric type I ($\alpha = \pi/30$) 	19.73	0.62	14.04	0.24	0.97
	Non-axisymmetric type II ($\alpha = 1.5\pi/20$) 	25.39	0.62	19.71	0.24	0.97
	Non-axisymmetric type III ($\alpha = 2\pi/15$) 	45.26	0.62	39.59	0.24	0.97

comparison with the acyl chain region, or a change of relative area between both bilayer leaflets [39]. The modified expression for the elastic energy is given by

$$E = \int \left[\frac{k_c}{2} (c_1 + c_2 - c_0)^2 + \bar{k} c_1 c_2 \right] dA \quad (5)$$

where k_c and \bar{k} are elastic constants with values 2×10^{-19} J and 4×10^{-19} J [4] respectively, and c_0 is the spontaneous curvature. Note that k_c plays the role of the constant D in Canham's model. The contribution of the term $\bar{k} c_1 c_2$ to the integral over the closed RBC surface is a constant and thus independent of the cell surface. Therefore, in Eq. (5) only the term involving the spontaneous curvature is of interest to determine the shape with lower elastic energy. It is interesting to note that if we minimize the bending energy given by Eq. (5) with respect to the spontaneous curvature c_0 assumed to be constant on each surface, we find

$$c_0 = \frac{1}{A} \int (c_1 + c_2) dA \quad (6)$$









where A denotes the surface area of the corresponding cell shape and the surface integral must be calculated separately for the upper and the lower parts of the stomatocyte models. The values obtained for the spontaneous curvature for the different shapes are shown in Table 2. For the discocyte, the value $c_0 = 0.66 \mu\text{m}^{-1}$ is in good agreement with published results derived from experimental data [11,40]. The spontaneous curvature for the different types of stomatocyte decreases as the degree of invagination increases only while the cells maintain their elongated appearance. As the stomatocyte profile turns more spherical, the spontaneous curvature increases. Again, the spherostomatocyte turns out to be the most stable shape with a value of $c_0 = 0.73 \mu\text{m}^{-1}$, providing a new evidence of the irreversibility of this spherical shape. The lack of axial symmetry leads to lower values of spontaneous curvature, $c_0 = 0.62 \mu\text{m}^{-1}$, and it remains approximately constant for the different non-axisymmetric discocytes considered in this study.

A comparison between the energy for the zero spontaneous curvature (Eq. 4) and for the non-zero spontaneous curvature Eq. (5) shows a bending energy increment given by:

$$\Delta E_{\text{bending}} = c_0^2 A k_c / 2 \quad (7)$$

where A is the total area for each shape. The energies obtained for the geometries of the DS sequence and for the non-axisymmetric shapes

Table 3
Local bending energy term, non-local bending energy term and bending energy for the DS sequence and the non-axisymmetric shapes randomly observed.

Cell shape		Local bending energy ($\times 10^{-18}$ J)	Non-local bending energy ($\times 10^{-19}$ J)	Bending energy ($\times 10^{-18}$ J)
Axisymmetric shapes DS sequence	Sphero-stomatocyte 	0.94	10.5	1.99
	Stomatocyte type III 	11.78	4.69	12.25
	Stomatocyte type II 	16.06	2.62	16.32
	Stomatocyte type I 	10.05	0.17	10.07
	Discocyte 	4.00	0	4.00
Non-axisymmetric shapes	Non-axisymmetric type I ($\alpha = \pi/30$) 	14.04	0.70	14.11
	Non-axisymmetric type II ($\alpha = 1.5\pi/20$) 	19.71	0.66	19.78
	Non-axisymmetric type III ($\alpha = 2\pi/15$) 	39.59	0.61	39.65

are shown in Table 2. Again, in the discocyte–stomatocyte sequence, the type II stomatocyte has the highest energy, whereas the lowest value was obtained for the spherostomatocyte. The effect of loss of symmetry is even more significant than the deformation involved on DS sequence with higher values of bending energy.

All these results confirm the significant role that the spontaneous curvature plays on the outside–inside asymmetry of the leaflet composition, in particular when applied to axisymmetric and non-axisymmetric discocytes. As a preliminary conclusion, we could say that an incorrect estimation of elastic energy needed to deform the red blood cell is obtained if the effect of the spontaneous curvature is disregarded.

3.3. Local and nonlocal bending energy model

Thus far our calculations of bending energy are based only on the concept of curvature. Certainly, the energy model given by Eq. (5) includes not only the mean curvature (as the classical Canham energy model does) but also the spontaneous curvature, thus accounting for the fact that the two sides of the membrane may have different molecular compositions. However, this model neglects any effect arising from the finite membrane thickness, the other reason for membrane deformation. This effect may lead to significant changes in the relative areas, depending on the curvature but also on the thickness, needed to adjust the number of lipids on the two sides of the membrane. Therefore, it is of primary importance in determining the overall shape deformations in the discocyte–stomatocyte transformation to take into account the difference areas on both sides of the membrane. We consider in this section a more complete energy model characterized not only by a bending rigidity and a spontaneous curvature, but also by an area-difference-elasticity (ADE) term [41–44]. This new term accounts for the difference in relaxed area between the outer and inner leaflets:

$$E = E_{\text{local}} + E_{\text{non-local}} \quad (8)$$

$$E_{\text{local}} = \frac{k_c}{2} \int_A (c_1 + c_2 - c_0)^2 dA \quad (8a)$$

$$E_{\text{non-local}} = \frac{\bar{k}}{2Ad^2} (\Delta A - \Delta A_0)^2. \quad (8b)$$

The first term is referred as the *local* bending energy contribution, whereas the second term, the ADE term, also referred as the *non-local* bending energy, is a function of the surface area A , the distance between the neutral surfaces of the leaflets, the non-local bending energy modulus \bar{k} , the relaxed area difference ΔA_0 and the area difference ΔA required by the two leaflets of a closed bilayer of fixed interleaf separation d . Assuming that d is small, the area difference ΔA as a function of the principal curvatures is

$$\Delta A = d \int dA (c_1 + c_2). \quad (9)$$

The ADE term represents the amount of stretching energy required by the two individual leaflets to conform to the deformed shape from a relaxed reference area difference ΔA_0 . Unlike previous studies that considered a flat disk as the relaxed shape of the cell, we start off from the natural discocyte geometry of the RBC surface, i.e., we study the evolution from the RBC resting shape. To determine the non-local energy contribution given by Eq. (8b), we first use Eq. (9) to calculate our discocyte reference value, which turns out to be $\Delta A_0 = 0.25 \mu\text{m}^2$, and then ΔA for the altered shapes. In all these calculations we have used $d = 3$ nm, $\bar{k} = 4 \times 10^{-19}$ J [5], and the geometrical parameters of Table 1. The results shown in Table 2 indicate that the calculated values of ΔA and $\Delta A/\Delta A_0$ gradually decrease as the degree of concavity increases. We remark that the value obtained for ΔA_0 for the discocyte is lower than the one previously calculated by Beck [45] due to the

different choice of volume and area values for the discocyte model. We note that if we apply our proposed parameterization to model the discocyte studied by Beck, we obtain a value of $0.412 \mu\text{m}^2$ for ΔA , which is in good agreement with the value of $0.41 \mu\text{m}^2$ estimated by Beck. As it is shown in Table 2, a general tendency was found for the value of ΔA for the different shapes of the DS transformation, at the beginning of the sequence the value remains constant but it decreases as the shape turns out more spherical. This result was partially shown by Beck although it must be noted that his study only showed an elongated stomatocyte similar to our model type II, and therefore his value of ΔA for the stomatocyte was of $0.39 \mu\text{m}^2$, slightly lower than the one ($0.41 \mu\text{m}^2$) obtained for its discocyte model.

Table 3 shows the local and non-local contributions to the bending energy as well as the total elastic energy for the cells of the DS sequence. Except for the spherostomatocyte, we see that the contribution of the ADE term is at least an order of magnitude lower than the local energy value. The non-local value for the spherostomatocyte is even higher than the corresponding local term. We remark that although it is rather spherical, there is a noticeable effect of a concavity in the central body surface on the elastic energy in comparison with a spherical RBC. This result is due to the negative sign of the spontaneous curvature of the spherical shape. The results confirm the theory of the bilayer couple approach [23,46–48]. Namely, the mechanism for the RBC shapes involves small changes in the area difference between the two leaflets of the plasma membrane even without taking into account the shear energy of the membrane skeleton and the energy contribution due to non-homogeneous redistribution of the membrane components [7,8,49]. Thus, any effect that expands the inner leaflet relative to the outer one tends to form concavities to accommodate the extra area. These effects are significant for stomatocyte types II and III. However, the loss of axisymmetry in the discocyte does not have a significant effect on the corresponding nonlocal contribution. We also note that, during the evolution process, non-axisymmetric and the DS shapes show similar variations for the spontaneous curvature and the area difference. This is expected as both c_0 and ΔA derive from asymmetries in the membrane leaflets. The results show that either a decrease on spontaneous curvature, a higher degree of concavities or an increase on the area difference may lead to a higher value of the elastic energy.

4. Discussion

We have performed a systematic quantitative analysis of the elastic energy of different cell shapes observed during the discocyte–stomatocyte sequence. For this purpose, we have derived parametric equations that reproduce the cell shapes. Our parameterizations can model both healthy and deformed RBCs (such as the *P. falciparum*-invaded RBCs considered in [17]), and therefore complement the method of [17], which provides a complete calculation of the mechanical parameters such as the membrane shear modulus, the linear elastic area compression modulus, or the Young's modulus. Moreover, these parameterizations can be used to generate initial approximations for purely numerical schemes that may elucidate the presence of local minima in a very complex elastic energy landscape.

We have confirmed that the simple energy model proposed by Canham overestimates the total energy for the shapes in discocyte–stomatocyte sequence. We then used a more complete energy model that included the local and non-local contributions to the total energy. However, unlike the previous studies that considered a flat disk as the relaxed shape of the cell, we start off from the natural discocyte geometry of the RBC surface to accurately reflect the evolution from the RBC resting shape. The value of the spontaneous curvature calculated for the discocyte is in very good agreement with the values published in previous studies. The results show that the non-local energy contribution is considerably lower than the local contribution for the different shapes of the DS sequence and that the local energy for the different shapes is always higher than the corresponding to the equilibrium biconcave

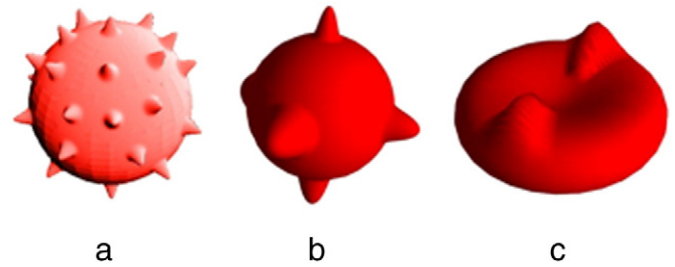


Fig. 3. 3D models of crenated RBC cells: a) echinocyte, b) acanthocyte and c) keratocyte.

shape. So we may conclude that bending energy of any of the studied altered RBC shape is higher than the resting biconcave geometry.

We have also analyzed the spherostomatocyte, for which we found a noticeable effect of a concavity on the central body surface in comparison with the energy of a spherical RBC.

As a possible line of development of the present work we mention the study of crenated cells, a generic term used to embrace the different shapes that show protuberances or spicules over the surface of one of the RBCs of the main sequence. More specific terms such as echinocyte, acanthocyte and keratocyte have been proposed by Bessis [4] to refer to certain types of these abnormal cells, which have been studied by scanning electron microscopy. Several authors [26–31] have presented different mathematical models for the spicules, some of which lead to non-smooth surfaces [50]. In our approach of using parametric representations of the surfaces with a small number of parameters, we can circumvent this problem by modeling spicules to be superimposed to the normal surface using a smooth function with compact support, so that the junction of the spicule to the spherical surface is smooth. For example, by multiplying the third component of one of the previous parameterizations given in Eqs. (2) and (3) by functions of the form

$$s(u, \phi) = 1 + h \exp \left[-1 / \left(\Delta \phi^2 - (\phi - \phi_0)^2 \right) + 1 / \Delta \phi^2 \right] \exp \left[-1 / \left(\Delta u^2 - (u - u_0)^2 \right) + 1 / \Delta u^2 \right] \quad (10)$$

we can add spicules of height h and widths (in two orthogonal directions) given by $\Delta \phi$ and Δu respectively. In this way we have generated the different shapes in Fig. 3. However, in most of these shapes, especially with thin spicules, the contribution of the shear energy of the membrane skeleton and the energy contribution due inhomogeneous distribution of membrane components [6,7,49] cannot be neglected (as can be to our degree of accuracy in the shapes of the discocyte–stomatocyte sequence), and a new ordering principle is required to compare the energies of the different shapes.

Acknowledgments

The financial support of UCM-Santander to Bioelectromagnetism Research Group 910305 and of Ministerio de Ciencia e Innovación Project nº FIS 2011-22566 is gratefully acknowledged.

References

- [1] G. Gompper, M. Schick, *Soft Matter: Lipid Bilayers and Red Blood Cells*, vol. 4, Wiley-VCH Verlag GmbH & Co. KGaA, 2008.
- [2] B.S. Bull, J. Brailsford, The biconcavity of the red cell: an analysis of several hypotheses, *Blood* 41 (1973) 833–844.
- [3] S.V. Rudenko, Erythrocyte morphological states, phases, transitions and trajectories, *Biochim. Biophys. Acta* 1798 (2010) 1767–1778.
- [4] M. Bessis, *Living blood cells and their ultrastructure*, translated by R. I. Weed, Springer-Verlag, New York Inc., 1973.
- [5] G. Lim, M. Wortis, R. Mukhopadhyay, Stomatocyte–discocyte–echinocyte sequence of the human red blood cell: evidence for the bilayer-couple hypothesis from membrane mechanics, *Proc. Natl. Acad. Sci.* 99 (2002) 16766–16769.

- [6] B. Isomaa, H. Hägerstrand, G. Paatero, Shape transformations induced by amphiphiles in erythrocytes, *Biochim. Biophys. Acta* 899 (1987) 93–103.
- [7] R. Mukhopadhyay, G. Lim, M. Wortis, Echinocyte shape: bending, stretching and shear determine spicule shape and spacing, *Biophys. J.* 82 (2002) 1756–1772.
- [8] A. Iglič, V. Kralj-Iglič, H. Hägerstrand, Stability of spiculated red blood cells induced by intercalation of amphiphiles in cell membrane, *Med. Biol. Eng. Comput.* 36 (1998) 251–255.
- [9] R. Mukhopadhyay, G. Lim, M. Wortis, Echinocyte shapes: bending, stretching and shear determine spicule shape and spacing, *Cond-mat/0108122v2 [cond-mat.soft]* 2001. 1–27.
- [10] R.E. Waugh, Elastic energy of curvature-driven bump formation on red blood cell membrane, *Biophys. J.* 70 (1996) 1027–1035.
- [11] P.B. Canham, The minimum energy of bending as a possible explanation of the biconcave shape of the human red blood cell, *J. Theoret. Biol.* 26 (1970) 61–81.
- [12] H.S. Lew, Electro-tension and torque in biological membranes modeled as a dipole sheet in fluid conductors, *J. Biomech.* 5 (4) (1972) 399–408.
- [13] E.A. Evans, Bending resistance and chemically induced moments in membrane bilayers, *Biophys. J.* 14 (1974) 923–931.
- [14] H.J. Deuling, W. Helfrich, Red blood shapes as explained on the basis of curvature elasticity, *Biophys. J.* 36 (1976) 861–868.
- [15] E.A. Evans, Bending elastic modulus of red blood cell membrane derived from buckling instability in micropipette aspiration tests, *Biophys. J.* 43 (1983) 27–30.
- [16] M. Bessis, Red-cell shapes illustrated classification and its rationale, *Nouv. Rev. Fr. Hematol.* 12 (1972) 721–746.
- [17] M. Dao, J. Li, S. Suresh, Molecularly based analysis of deformation of spectrin network and human erythrocyte, *Mater. Sci. Eng. C* 26 (2006) 1232–1244.
- [18] D. Kabaso, N. Bobrovska, W. Gózd, N. Gov, V. Kralj-Iglič, P. Veranič, A. Iglič, On the role of membrane anisotropy and BAR proteins in the stability of tubular membrane structures, *J. Biomech.* 45 (2012) 231–238.
- [19] Q. Du, C. Liu, X. Wang, Simulating the deformation of vesicle membranes under elastic bending energy in three dimensions, *J. Comput. Phys.* 212 (2006) 757–777.
- [20] Q. Liu, Z. Haijun, J. Liu, O. Can, Spheres and prolate and oblate ellipsoids from an analytical solution of the spontaneous curvature fluid-membrane model, *Phys. Rev. E* 60 (3) (1999) 3227–3233.
- [21] S. Wolfram, *The Mathematical Book*, Seventh ed. Wolfram Media, 2008.
- [22] E. Evans, R. Skalak, *Mechanics and Thermodynamics of Biomembranes*, CRC Press, Boca Raton, Florida, 1980.
- [23] M.B. Hägerstrand, H. Hägerstrand, A. Iglič, Membrane skeleton and red blood cell vesiculation at low pH, *Biochim. Biophys. Acta* 1371 (1998) 123–128.
- [24] S. Muñoz, J.L. Sebastián, M. Sancho, G. Álvarez, Modelling normal and altered human erythrocyte shape by a new parametric equation: application to the calculation of induced transmembrane potentials, *Bioelectromagnetics* 25 (2006) 631–633.
- [25] S. Muñoz, J.L. Sebastián, M. Sancho, G. Martínez, Analysis of radiofrequency energy stored in the altered shapes: stomatocyte-echinocyte of human erythrocytes, *Bioelectrochem.* 77 (2010) 158–161.
- [26] J.L. Sebastián, S. Muñoz, M. Sancho, G. Álvarez, Polarizability of shelled particles of arbitrary shape in lossy media with an application to hematic cells, *Phys. Rev. E* 78 (2008) 1–11 (051905).
- [27] P.W. Kuchel, E.D. Fackrell, Parametric-equation representation of biconcave erythrocytes, *Bull. Math. Biol.* 61 (1999) 209–220.
- [28] S. Chien, S.A. Luse, C.A. Bryant, Hemolysis during filtration through micropores: a scanning electron microscopic and hemorheologic correlation, *Microvasc. Res.* 3 (1971) 183–203.
- [29] P.B. Canham, A.C. Burton, Distribution of size and shape in populations of normal human red cells, *Circ. Res.* 22 (1968) 405–422.
- [30] R.I. Weed, M. Bessis, The discocyte-stomatocyte equilibrium of normal and pathologic red cells, *Blood* 41 (1973) 471–475.
- [31] L.D. Landau, E.M. Lifshitz, *Theory of Elasticity*, translated by Sykes, J. B. and Reid, W. H. Pergamon Press, Oxford, 1970.
- [32] R.E. Waugh, R.G. Bauserman, Physical measurements of bilayer-skeletal separation forces, *Ann. Biomed. Eng.* 23 (1995) 308–321.
- [33] M.A. Lombolt, B. Loubetand, J.H. Ipsen, Elastic moderation of intrinsically applied tension in lipid membranes, *Phys. Rev. E* 83 (2011) 1–4 (011913).
- [34] E. Evans, D. Needham, Physical properties of surfactant bilayer membranes: thermal transitions, elasticity, rigidity, cohesion and colloidal interaction, *J. Phys. Chem.* 91 (1987) 4219–4228.
- [35] Y.C.B. Fung, P. Tong, Theory of the spherizing of red blood cells, *Biophys. J.* 8 (1968) 175–198.
- [36] W. Helfrich, Elastic properties of lipid bilayers: theory and possible experiments, *Z. Naturforsch.* 28c (1973) 693–703.
- [37] J.K. Khodadad, R.E. Waugh, J.L. Podolski, R. Josephs, T.L. Steck, Remodeling the shape of the skeleton in the intact red cell, *Biophys. J.* 70 (1996) 1036–1044.
- [38] R.E. Waugh, Elastic energy of curvature-driven bump formation on red blood cell membrane, *Biophys. J.* 70 (1996) 1027–1035.
- [39] N. Mohandas, A.C. Greenquist, S.B. Shohet, Bilayer balance and regulation of red cell shape, *J. Supramol. Struct. Cell. Biochem.* 9 (1978) 453–458.
- [40] E. Evans, Y.C. Fung, Improved measurements of the erythrocyte geometry, *Microvasc. Res.* 4 (1972) 335–347.
- [41] W.C. Hwang, R.E. Waugh, Energy of dissociation of lipid bilayer from the membrane skeleton of red blood cells, *Biophys. J.* 72 (1997) 2669–2678.
- [42] E.A. Evans, Y.C. Fung, Improved measurements of the erythrocyte geometry, *Microvasc. Res.* 4 (1972) 335–347.
- [43] E.A. Evans, Bending resistance and chemically induced moments in membrane bilayers, *Biophys. J.* 14 (1974) 923–931.
- [44] K.J. Khairy, J. Howard, Shapes of red blood cells: comparison of 3D confocal images with the bilayer-couple model, *Cell. Mol. Bioeng.* 1 (2–3) (2010) 173–181.
- [45] J.S. Beck, Relations between membrane monolayers in some red-cell shape transformations, *J. Theor. Biol.* 75 (1978) 487–501.
- [46] S. Svetina, M. Brumen, B. Zeks, Lipid bilayer elasticity and the bilayer couple interpretation of red cell shape transformations and lysis, *Stud. Biophys.* 110 (1985) 177–184.
- [47] M.P. Sheetz, S.J. Singer, Biological membranes as bilayer couples. A molecular mechanism of drug-erythrocyte interactions, *Proc. Natl. Acad. Sci.* 71 (1974) 4457–4461.
- [48] E.A. Evans, P.L. La Celle, Intrinsic material properties of the erythrocyte membrane indicated by mechanical analysis of deformation, *Blood* 45 (1975) 29–43.
- [49] H. Hägerstrand, L. Mrowczynska, U. Salzer, R. Prohaska, K.A. Michelsen, V. Kralj-Iglič, A. Iglič, Curvature-dependent lateral distribution of raft markers in the human erythrocyte membrane, *Mol. Membr. Biol.* 23 (2006) 277–288.
- [50] T.J. Larkin, P.W. Kuchel, Mathematical models of naturally “morphed” human erythrocytes: stomatocytes and echinocytes, *Bull. Math. Biol.* 72 (2010) 1323–1333.